THE STRUCTURE AND EVOLUTION OF A SOLAR FLARE AS OBSERVED IN 3.5–30 keV X-RAYS

R. A. HARRISON and G. M. SIMNETT
Department of Space Research, University of Birmingham
and
P. HOYNG, H. LaFLEUR, and H. F. VAN BEEK
The Astronomical Institute at Utrecht

(Received 28 May; in revised form 21 September, 1982)

Abstract. On July 5, 1980 the Hard X-Ray Imaging Spectrometer on board the Solar Maximum Mission observed a complex flare event starting at 22 : 32 UT from AR 2559 (Hale 16955), then at N 28 W 29, which developed finally into a 2-ribbon flare. In this paper we compare the X-ray images with Hα photographs taken at the Big Bear Solar Observatory and identify the site of the most energetic flare phenomena. During the early phases of the event the hard X-rays (> 16 keV) came from a compact source located near one of the two bright Hα kernels; we believe the latter are at the footpoints of a compact magnetic loop. The kernel identified with the X-ray source is immediately adjacent to one of the principal sunspots and in fact appears to 'rotate' around the sunspot over 90° in the early phase of the flare. Two intense X-ray bursts occur at the site of the rotating kernel, and following each burst the loop fills with hot, X-ray emitting plasma. If the first burst is interpreted as bremsstrahlung from a beam of electrons impinging on a collisionally dominated medium, the energy in such electrons, > 16 keV, is $\sim 5 \times 10^{30}$ erg. The altitude of the looptop is $7-10 \times 10^3$ km. The temperature structure of the flare is extremely non-homogeneous, and the highest temperatures are found in the top of the loop.

A few minutes after the hard X-ray bursts the configuration of the region changes; some of the flare energy is transferred along a system of larger loops that now become the defining structure for a 2-ribbon flare, which is how the flare develops as seen in Hα. In the late, cooling phase of the flare 15 min after maximum, we find a significant component of the plasma at temperatures between 25 and 30×10^6 K.

1. Introduction

With the launch of the Hard X-Ray Imaging Spectrometer (HXIS) on the Solar Maximum Mission (SMM) it became possible to study for the first time the spatial development of a solar flare in hard X-rays, above 10 keV, and to relate such measurements to Hα emission. One of the first results from HXIS was the identification of the site of the impulsive hard X-ray bursts observed at the onset of major flares (Hoyng *et al.*, 1981; Duijveman *et al.*, 1982). Frequently, in a large flare, the hot X-ray emitting plasma generated during and following the impulsive phase expands and obliterates any fine structure that might give a clue to the detailed development of the flare. We report here results from the study of an intense, but compact, flare where the structure of the X-ray emitting features has been identified throughout most of the event. It reveals a wealth of detail that cannot be conceived from a study of spatially unresolved X-ray data. Such studies alter significantly the picture we formerly held regarding the early stages of flare development. In our analysis we have made detailed comparisons with the Hα photographs from the Big Bear Solar Observatory.

Solar Physics **84** (1983) 237–261. 0038–0938/83/0842–0237$03.75.

The active region, (Boulder 2550, Hale 16955) was first identified as a new region on July 2, 1980 and from July 4 to July 8 it was the most active region on the visible solar disc. On July 3 and 4 it grew in magnetic complexity and by July 5 it had a high probability of flaring; from 13 : 00 UT on that day it was observed by HXIS. Between 13 : 06 and 24 : 00 UT HXIS recorded three events, of which the largest and best studied was the class 1B flare at 22 : 32 UT; this flare reached M 8.9 in the GOES soft X-ray classification and was monitored continuously by the Big Bear Solar Observatory in various parts of the Hα line. It was selected by us for detailed analysis because of the compact nature of X-ray emission over its entire history. The source of the X-ray emission could be identified with a particular flaring loop, invisible in Hα except for two bright kernels presumed to be the footpoints. Following each of the two main hard X-ray bursts, the 3.5–5.5 keV X-ray emission gradually increased throughout the loop. In the first burst, the footpoint opposing the site of the primary energy release became the brightest within approximately 80 s; in the second burst, the brightest element remained at the primary site for around 9 min. This timing is strongly energy dependent. Detailed analysis of the temperature structure is the subject of Simnett and Harrison (1982).

The magnetic configuration of the flare region was a classic δ with the following (f) and preceding (p) sunspots within the same umbra (see Figure 2f). The magnetic development has been discussed in detail by Zirin and Tanaka (1981) who describe continual spot changes within the umbra resulting in what they interpret as sheared field lines across the magnetic neutral line. As the flare evolved a very bright Hα kernel appeared to rotate about one of the p spots, and coincident with the position of the kernel a magnetic transient was observed (Zirin and Tanaka, 1981). It appeared as a single magnetic pole, which peaked at the time of the first hard X-ray burst and lasted for about 10 min; the data did not show a dipole but could not eliminate this possibility. The main energy release occurred about the same time as the observed peak in the magnetic transient. As the flare evolved further there was a sudden change in the Hα emission which manifested itself by an apparent breaking of bright plage around the sunspot, followed by re-connection on the opposite side of the spot; simultaneously a bright Hα ribbon linked two of the p spots in this active region. We believe this event signals a critical development in the expansion of the flare plasma within the complex magnetic fields, and correlate this with a change in the decay rates of the hard and soft X-rays.

In Sections 2 and 3 we outline the Hα and X-ray observations, respectively. In Section 4 we develop a model of the flare region consistent with the observations. Finally in Section 5 we derive quantitative physical parameters pertaining to the site of the main energy release.

2. The Hα Observations

We start by discussing the Hα observations because traditionally the majority of detailed analysis of flare morphology has been at this wavelength, and consequently such observations are familiar to a broad section of the community. This should enable the

reader to have a feeling for the nature of this flare before coming to the unfamiliar X-ray data. However, the most energetic flare processes produce plasmas which, initially, are too hot to be visible in Hα, and bremsstrahlung which has negligible power in the Hα region. Therefore the Hα is likely to be an end product of faster, hotter and more energetic processes (than those producing Hα directly) which can now be studied for the first time at wavelengths equivalent to 3.5–30 keV X-rays. The novel X-ray imaging data have characteristics which, because of their coarser spatial resolution make them harder to assimilate than optical photographs, and lend themselves to a different presentation. Therefore the discussion of the X-ray data in Section 3 attempts to introduce the reader to the new medium in the context of an energetic flare study.

Figure 1a shows the appearance of AR2550 at 22:30:37 UT in the blue wing (−0.5 Å) of Hα*, around 2 min prior to flare onset. Figure 1b identifies certain distinct parts of the region which are referred to in our subsequent discussions, and indicates the position of the magnetic polarity inversion line (shown dotted) between the main group of sunspots. A sunspot picture, taken in 1 Å off band Hα, is shown in Figure 2f. The group of *p* spots is to the SE of the line, and the *f* spots to the NW.

Before the main flare under discussion here took place, there was some activity which we have found useful for checking the alignment of the HXIS field of view with respect to the active region. At 16:02 UT a small, SB flare developed as two bright ribbons on either side of the neutral line with a strong enhancement to the south west, close to sunspot *F*. This implies good communication between the main group of sunspots and spot *F*, a distance of 2′, or 160000 km at this latitude and longitude. After 18:36 UT, a small bright Hα patch developed to the NW of sunspot *A*. Both events produced X-ray emission in the 3.5–5.5 keV energy range imaged by HXIS. A discussion of this information for alignment purposes is given in the Appendix.

Around 19:30 UT a bright plage filament formed a bridge across sunspot *A* in an EW direction. The filament is visible in Figure 1a where it starts in a complex twist north of *D*, comes around between *D* and *C*, follows a path south to sunspot *A*, twists over *A* (the light bridge) and goes around between *A* and *B* before linking back to *C*. The initial phases of the flare appear in Hα at the points of greater apparent curvature of this filament both around *A* and to the north of *D*. The light bridge evolved from the bright Hα patch seen at 18:36 UT. Following the initial trigger, the intense Hα emission along the light bridge migrated to the south of *A* to form a bright Hα kernel. Simultaneously a less intense kernel formed to the NE of *B*, and appeared to represent one end of a diverging arcade of magnetic loops which extended to the NW of *D*. The appearance of the region at 22:35:57 UT is illustrated in Figure 2a. Note that the loop system is all to the north of the complicated bright filament discussed above.

By 22:39:46 UT (Figure 2b) the appearance of the bright kernel at *A* has completely changed; it appears to have consolidated and *rotated* 90° so that instead of being to the south of *A* it is now centered to the west of *A*. Furthermore, the kernel to the NE of

* The majority of the Hα observations used for this paper were taken in the blue wing of the Hα line at −0.5 Å. Henceforth this will be assumed in the discussion and only the notation, Hα, will be used.

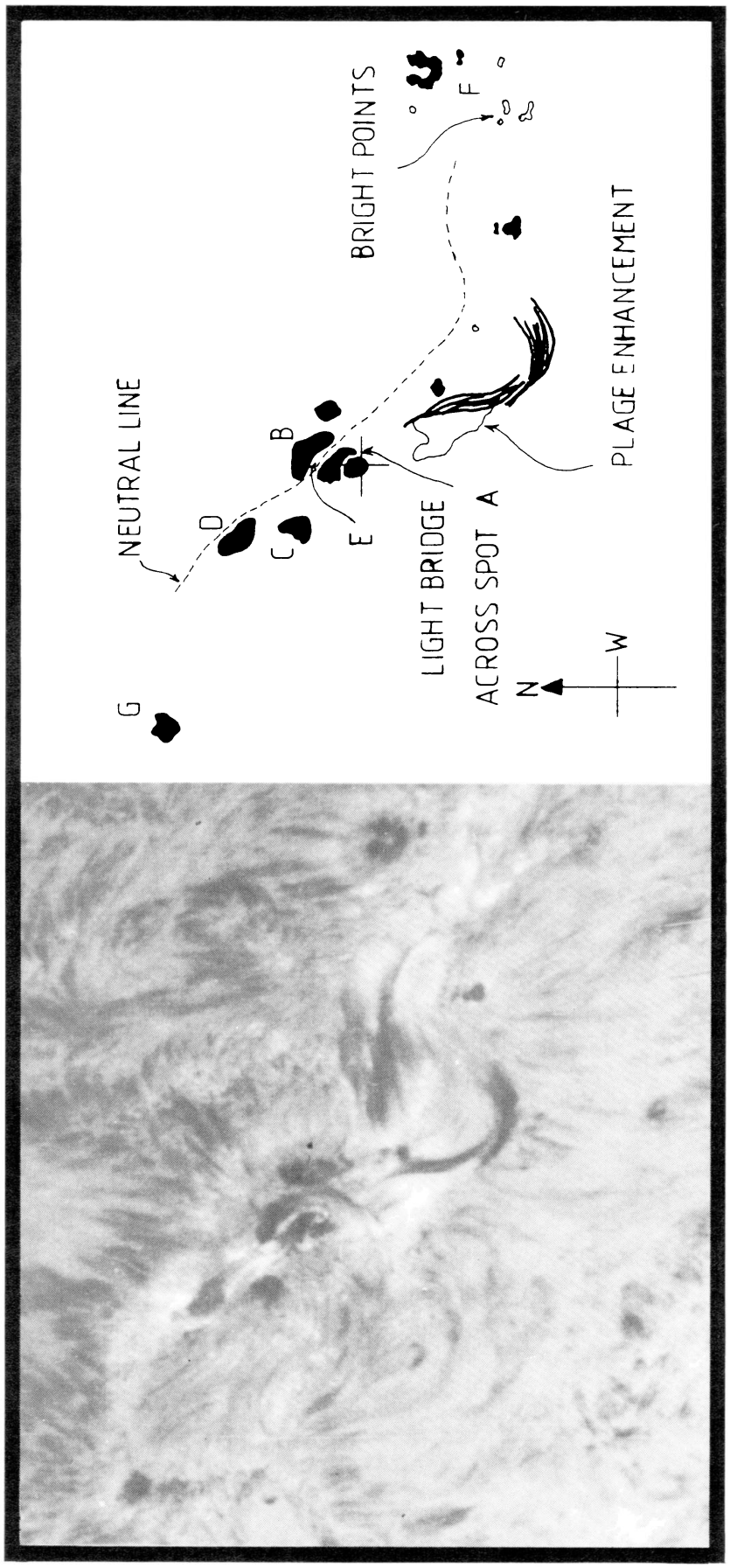

Fig. 1. (a) Hα photograph just prior to the flare onset. Note the bright twisted filament running through the region and crossing over one of the sunspots. (Courtesy of Big Bear Solar Observatory.) (b) A schematic representation of the sunspot region, identifying some principal features and showing the location of the centre of the HXIS field of view.

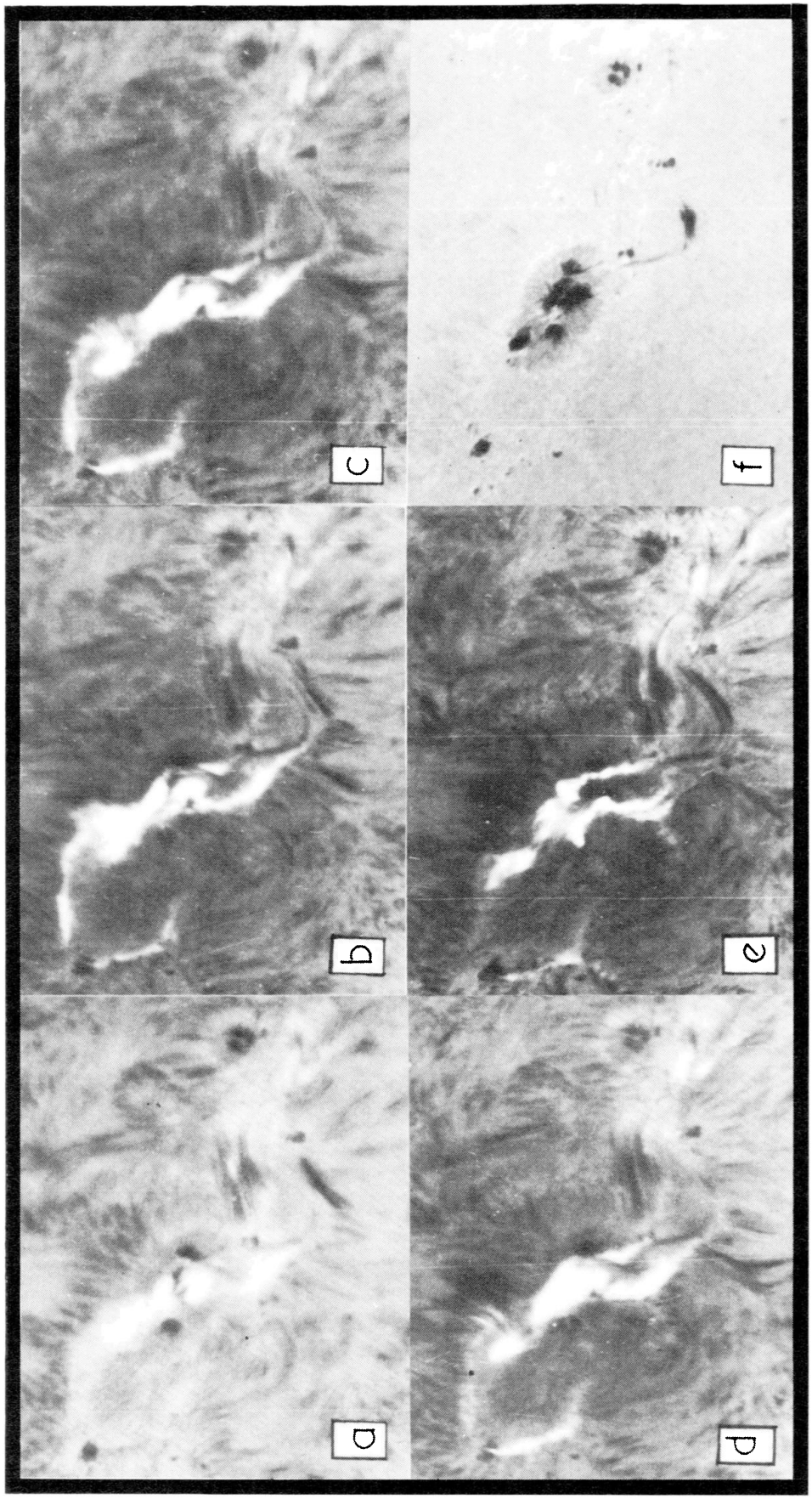

Fig. 2. Hα photographs throughout the flare: (a) 22:35:57 UT. (b) 22:39:46 UT. (c) 22:42:37 UT. (d) 22:44:32 UT. (e) 22:59:10 UT. (f) A sunspot photograph of the active region. (Coutesy of Big Bear Solar Observatory.)

B has strengthened, and the Hα emission from the loop system has both strengthened and expanded. As we shall show in the next section, it is at this time that the first major hard X-ray burst is observed. It also corresponds to the peak of the magnetic transient observed by Zirin and Tanaka (1981). There is a bright ribbon of enhanced plage extending from the northern locus of the primary loop footpoints around to *G*; and also a similar ribbon extending south from *A*.

By 22 : 42 : 37 UT the flare appearance has changed once again (Figure 2c). The main kernel to the west of *A* has extended towards the NE and the kernel to the NE of *B* has elongated in a direction towards *D*. Note that it is not extending along the northerly locus of the primary loop footpoints, but more along the southerly locus. Only faint Hα emission is visible from the looptops, probably indicating cooling. The site of the original twisted filament near *D* is now quite bright. The flare, for the first time, is beginning to look like a 2-ribbon flare.

Figure 2d shows the flare at 22 : 44 : 32 UT, by which time it is quite apparent that the NW ribbon is extending towards *D*. The primary loop system now seems detached from the rest of the flare, and as the loops fade the bright plage extending around to *G* also fades. The other change is in the direction of expansion of the bright kernel around *A*, which had appeared to be moving towards *D* through the apparent point of crossing of the preflare twisted filament; it now starts to separate from the NW ribbon. At 22 : 47 : 30 UT the kernel around *A* breaks from the bright plage extending south from *A*; it moves eastwards across the northern edge of *A* and rejoins the plage to the eastern edge of the spot. At the same time this ribbon links directly to sunspot *C*. The late stage of the flare, showing these changes, is illustrated in Figure 2e, taken at 22 : 59 : 10 UT. In this picture there is clearly a new system of (secondary) loops visible, spanning the two ribbons, with the loop tops emitting quite strongly in Hα.

The conclusion we draw from the Hα pictures is that throughout the course of the flare the region has changed. During the initial phases, there is not Hα associated with sunspot *C* and the complex structure around and the ribbon moving around to *G*. Yet by the end of the flare, there are simply two ribbons linking *A* to *C*, and *B* to *D*, with bright post flare (secondary) loops across them. We now turn to the X-ray observations, to identify the site of the main energy releases.

3. The Hard X-Ray Observations

A description of HXIS has been published elsewhere (Van Beek *et al.*, 1980). The current analysis uses images with a nominal 8″ spatial resolution, accumulated simultaneously over the six energy bands 3.5–5.5–8.0–11.5–16–22–30 keV, and with a time resolution of either 3.1 s or 9.2 s, depending on the phase of the flare. The duty cycle of HXIS during this event was 50%, so each image was accumulated over a time equal to one half of the stated time resolution. The flare was in progress at orbit dawn (22 : 37 : 4 UT), but the main phase of the hard X-ray activity (22–30 keV) took place after 22 : 39 UT. The intensity-time history of the 22–30 keV X-ray intensity for the total HXIS field of view, of 6′24″ × 6′24″, including the High Energy Monitor (see Van

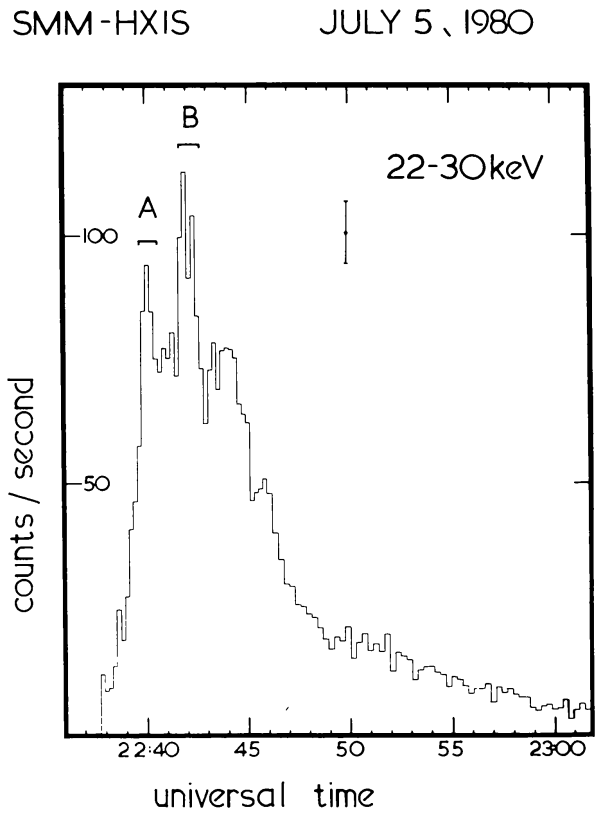

Fig. 3. The intensity-time profile of the 22–30 keV X-ray intensity from the full HXIS field of view. The typical statistical uncertainty at the height of the burst is indicated. Two features of the burst are identified, *A*, *B*. Note the change in decay at 22:47 UT.

Beek *et al.*, 1980) is shown in Figure 3. Two periods *A* and *B*, are identified where the time structure and spectral evolution appear to reflect the impulsive release, or deposition, of energy. In fact these are the more significant of a number of discrete bursts with similar rise and fall times, consistent with the elementary flare bursts discussed by de Jager and de Jonge (1978). Note that the decay rate changes around 22:47 UT. The X-ray spectrum at this time does not exhibit any sudden changes; therefore we rule out any fresh impulsive energy release. More likely the flare plasma breaks out into a different part of the flare region, and the high energy electrons producing the X-rays are contained in a much larger volume at low density and consequently have a longer lifetime. This is discussed in more detail in Section 4.

Figure 4 shows the intensity-time history for the energy interval 3.5–5.5 keV. The fine time structure seen at higher energies is completely lacking with maximum intensity being reached several minutes after the intense hard X-ray features. This is exactly what would be expected based on previous solar X-ray studies; however, when the full imaging capability of HXIS is used, a rather complex picture emerges.

We will discuss the flare first using the 16–30 keV images, as these X-rays probably originate from the electrons accelerated at the times of the primary energy releases. Figure 5 is a 3-dimensional spatial-intensity-time map of the 16–30 keV X-rays. Each of the numbered boxes represents the light curve for one 8″ × 8″ pixel and Figure 6

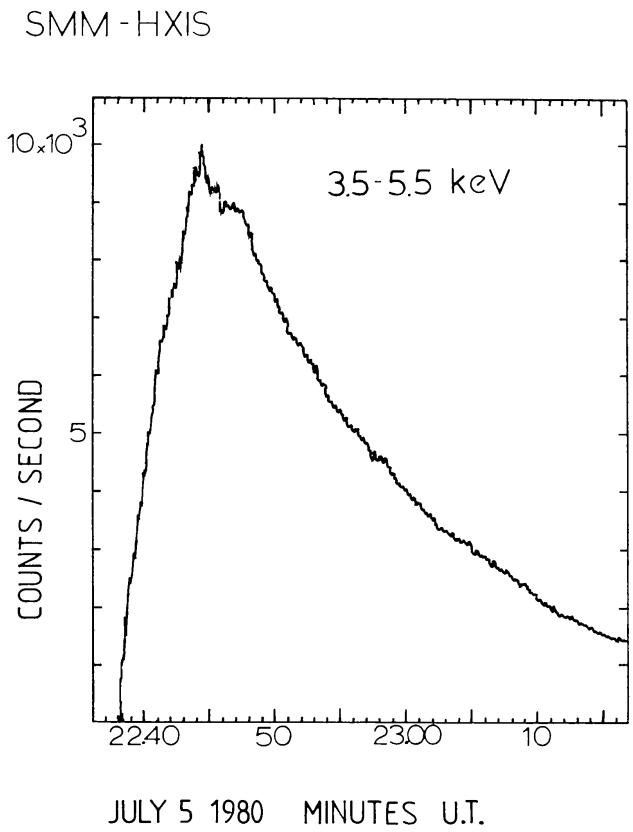

Fig. 4. The intensity-time profile of the 3.5–5.5 keV X-ray intensity from the whole flare region. Note the change in decay at 22:47 UT.

shows the projected locations of these pixels on a reproduction of the active region taken from Figure 1a. The alignment is accurate to $\sim 5''$ and details of the alignment procedure are given in the Appendix. The pixels are assigned numbers which refer to their position in the detector array; these numbers have no other significance. Note that the pixels shown on Figure 5 represent only that part of the HXIS field of view containing the flare; the remainder of the field of view is omitted to simplify the figure. The activity is concentrated in the area shown (see Figure 6), as is demonstrated by the intensity-time history for pixel No. 313, which represents an $8'' \times 8''$ area to the west of No. 293. Pixel No. 313 has the highest intensity of all those *surrounding* the area covered by Figure 5. Data from individual pixels before 22:38:25 UT is not useful as the SMM spacecraft underwent a minor corrective slew of $\sim 2''$ to compensate for drift during orbit night. The slew does not affect the total field of view light curves significantly.

It is immediately apparent from Figure 5 that the flare in hard X-rays is extremely compact, and furthermore that the adjacent pixels with the highest rates do not have similar light curves. The major part of the flare is contained within pixels No. 272, No. 273, No. 292, and No. 293. Figure 7 shows an expanded and time-averaged plot of the data from these pixels from which the following points can be established:

(1) During the first burst, *A*, the emission is primarily from No. 272 with a significant amount in No. 292, to the west. Reference to Figure 5 shows that at the onset of this burst there is a high intensity also from No. 271 to the south.

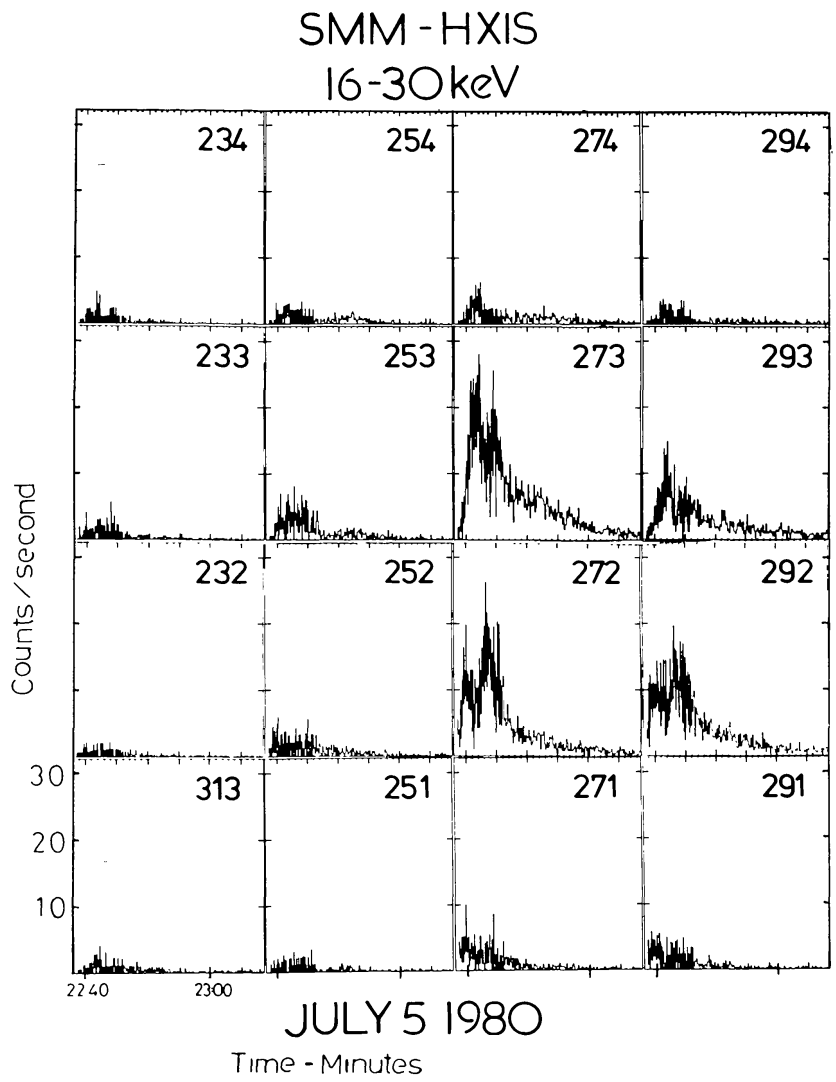

Fig. 5. A three-dimensional spatial-intensity-time map of the hard X-ray flare. Each numbered plot is an individual intensity-time profile of one 8″ × 8″ pixel. The relative location of the pixels in the flare region is shown in Figure 6. The intensity-time axes are the same for each individual plot. North is up and west is right.

(2) During period *B* the emission is primarily from No. 273, although the emission from No. 293 also reaches a maximum at this time.

(3) During period *B* the intensity in No. 272 increases, the increase being more marked towards the end of the period. The intensity in No. 273 and No. 293, however, rises to a maximum in the first half of period *B*, and subsequently falls. Thus we may state with confidence that at least part of burst *B* is from these pixels. The decay of burst *A*, however, is arrested in No. 272 prior to period *B*, so it is plausible that the profile in No. 272 is the superposition of the true decay of *A* plus a similar burst to that seen in No. 273 and No. 293. This hypothesis is supported by the fact that the energy spectrum of No. 272 suddenly changes at the onset of *B*.

At this point we wish to introduce briefly the scenario we envisage to explain these data, as it should aid the comprehension of the remainder of the data. The sequence of events is as follows: a hard X-ray burst (*A*) appears in No. 272 (plus to a lesser degree

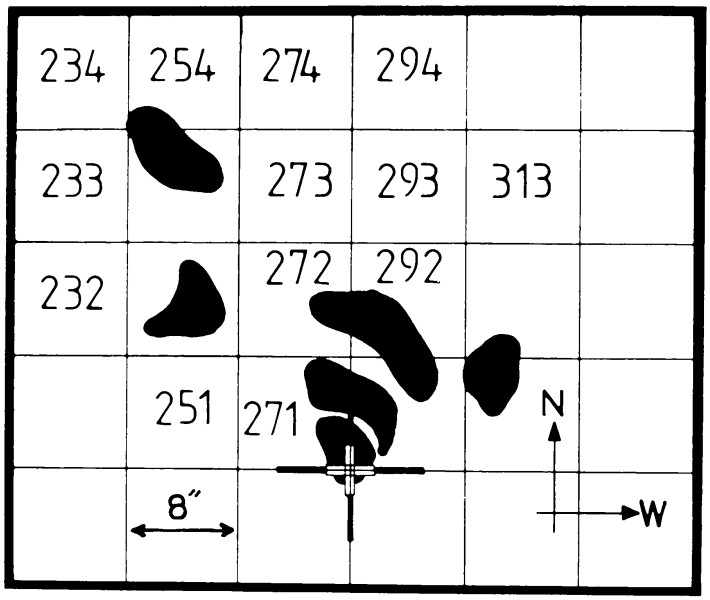

Fig. 6. A map showing the position of the pixels in Figures 5 and 9 relative to the active region. The features of the region are identified in Figure 1b. Pixel 291 is directly to the south of pixel 292.

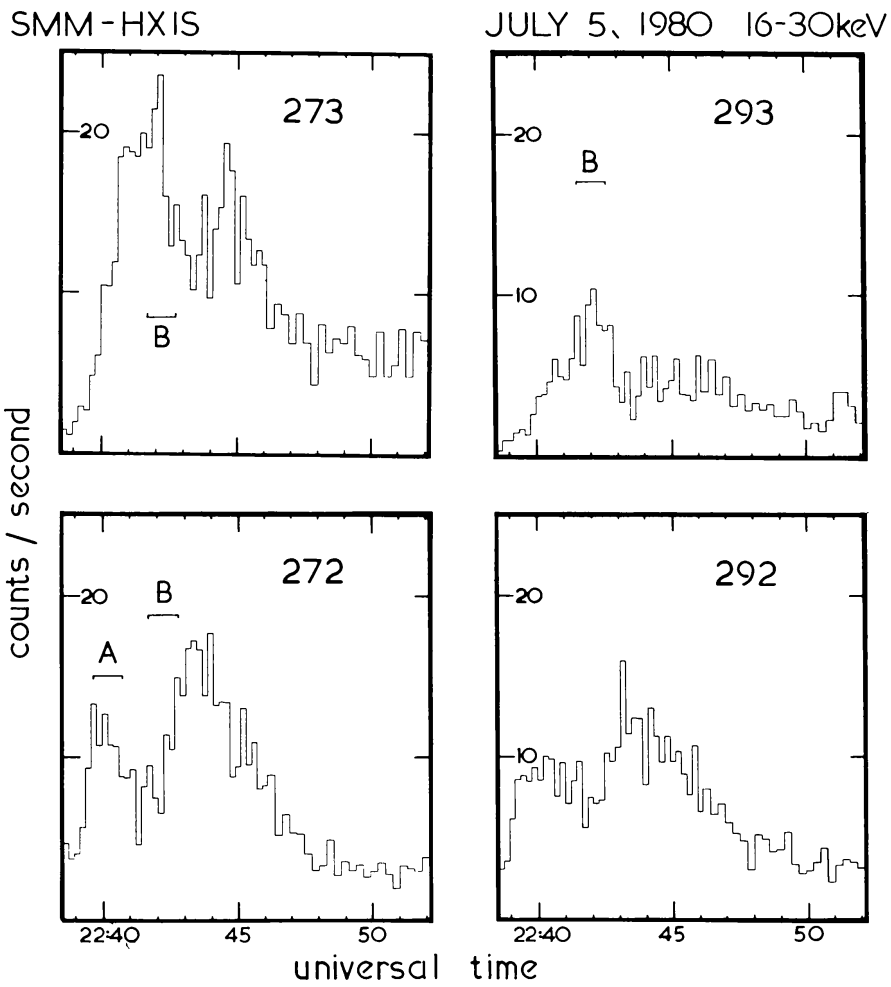

Fig. 7. An expanded and time averaged plot of the four brightest pixels in the hard X-ray flare. The times of bursts *A* and *B* are indicated (see Figure 3).

in No. 292) following which the hard X-ray emission in No. 292 and No. 273 gradually rises, even after the burst in *A* has subsided. A second burst, *B*, appears simultaneously (within the time resolution of Figure 7) over No. 272, No. 293, and No. 273, followed immediately in No. 272 by a gradual increase in emission which lasts until 22 : 44 UT. As this decays the intensity in No. 273 increases. We interpret the *bursts* as originating as bremsstrahlung from non-thermal electrons and the *gradual* increases as thermal emission from the high temperature plasma resulting from the impulsive process that produced the *bursts*. There is a compact magnetic loop stretching from No. 272/292 to No. 273, the top of which is seen via projection in No. 293. We discuss this fully in Section 4.

We now demonstrate both the compact nature of the flare and the dramatic spatial evolution as seen by hard X-ray images. Figure 8 shows contour maps separately for the energy intervals 16–22 keV and 22–30 keV corrected for the triangular response of the HXIS collimator, for three different time intervals: 22 : 38 : 27–22 : 39 : 50, 22 : 40 : 58–22 : 42 : 00, and 22 : 42 : 48–22 : 43 : 50 UT. Note that the first two intervals cover the first part only of periods *A* and *B* (Figure 3). For the first period, at 16–22 keV, the burst is concentrated on the southern boundary of row 3, in columns 3 and 4, corresponding to No. 292 and No. 272. At 22–30 keV the core is in row 3 column 3

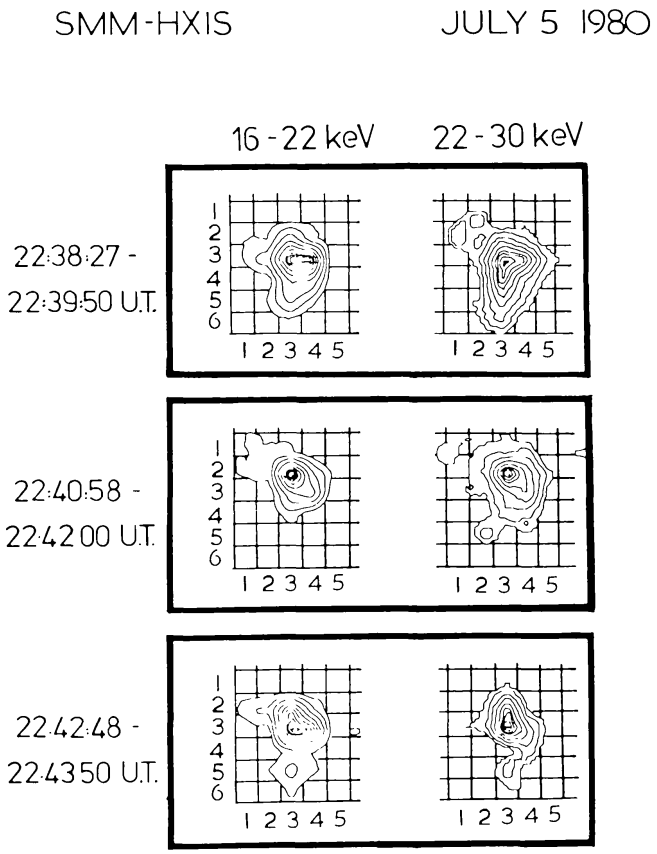

Fig. 8. Contour maps of the 16–22 keV and 22–30 keV X-ray intensities at three different times in the flare. The contour levels are at 98, 90, 80, 70, 55, 40, 26, 14, and 7%, with the addition of a 3% level in the 16–22 keV maps. The images are corrected for the triangular response of the collimator.

(No. 272) while the southerly extension is quite noticeable. This is a result of the onset of the burst appearing in No. 271. In the second period the core of the burst has shifted to the southern part of row 2, column 3 where it has a FWHM of 6″ in the 16–22 keV contour. The extension to the SW towards the site of the first burst is clearly visible. In the third period the core of the emission has moved back to the southern edge of row 3, column 3, or No. 272, with some extension both northwards to the site of the core in period 2 and to the west.

We now turn to the soft X-ray images, in the 3.5–5.5 keV energy interval. Figure 9 shows a similar three dimensional map to Figure 5. Some pixels are plotted at a reduced intensity scale and pixels No. 252 and No. 271 include a correction for space-charge effects. They are most pronounced when there is high contrast between adjacent pixels

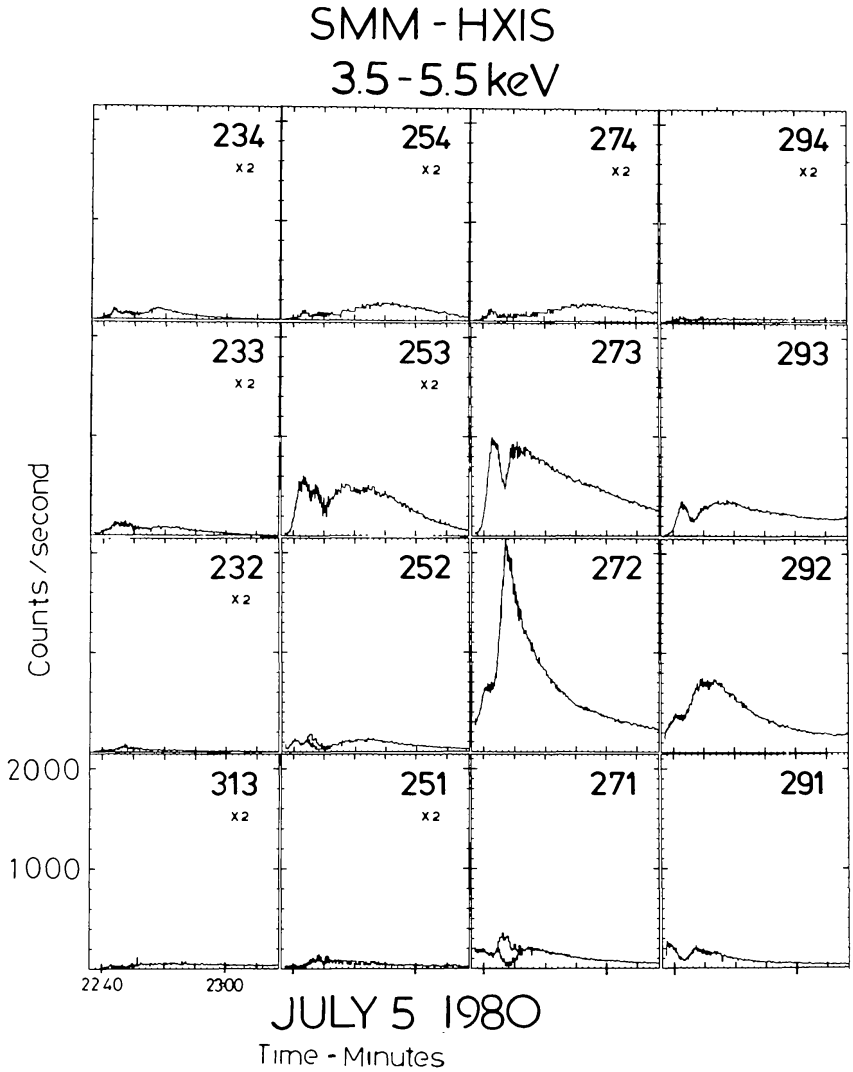

Fig. 9. A three-dimensional spatial-intensity-time map of the soft X-ray flare. Each numbered plot is an individual intensity-time profile of one 8″ × 8″ pixel. The relative location of the pixels in the flare region is shown in Figure 6. The intensity and time axes are the same for each individual plot, except for a two-fold magnification in intensity for pixels identified (× 2). Pixels 252 and 271 include a correction (upper line) between 22:42 and 22:46 UT to allow for space charge effects in the detector.

and affect primarily the lowest energies (Boelee, 1983). The remaining pixels are not believed to need any correction.

The soft X-ray core of the flare, prior to the hard X-ray burst, is in No. 272, No. 292, No. 271, and No. 291 such that the centroid is virtually at their point of intersection. Note the weak emission from No. 252 and No. 233, extending to the NE. The soft X-ray emission gradually rises in No. 272 and No. 292, approximately doubling by 22 : 40 UT when the level is 650 counts s^{-1} in No. 272 and 375 counts s^{-1} in No. 292. However, whereas the intensity in these pixels levels off, that in No. 273 continues to rise to a maximum of 1000 counts s^{-1} by 22 : 41 UT. The behaviour of No. 293 is virtually identical except at a lower intensity, this only reaching 330 counts s^{-1} at maximum. For the next few minutes, these bright pixels behave in opposite senses; while those to the south increase, those to the north decrease, and vice-versa. It is significant that the two dominant soft X-ray peaks, namely at 22 : 41 UT in No. 273 and 22 : 43 : 20 UT in No. 272, coincide with the hard X-ray maximum in these pixels, supporting our hypothesis (see above and Section 4) that the X-ray emission at these times is predominantly from a high temperature plasma.

A weak maximum is seen late in the event in some surrounding pixels. For example, the maximum in No. 254 is at 22 : 55 : 00 UT ±30 s; in No. 274 it is at 22 : 57 : 30 UT ±30 s; No. 252 it is at 22 : 52 : 30 UT ±30 s; in No. 234 it is at 22 : 48 : 50 UT ±20 s; whereas in No. 253 there are two maxima, the latest being at 22 : 53 : 00 UT ±30 s. We leave the discussion of this to the next section.

4. The Model of the Flare Region

In this section we discuss the flare at well identified phases of its development when we can observe the results of significant changes in the physical conditions governing its evolution. During the various stages we describe the features of the region which are most appropriate to fit the observations.

4.1. The period before 22 : 38 : 30 UT

Comparison of the hard X-ray data with the Hα data shows that before any substantial fraction of the 22–30 keV X-rays was produced the flare had already developed in two places. The more intense region was coincident with the location of the bright filament which previously formed the light bridge across sunspot *A*; whereas the more extensive region started in a small kernel to the NE of *B*, expanding into a magnetic loop system reaching to the north of *D* (see Figure 1b). During this early phase, the X-ray spectrum from the core of the flare, pixels 271, 272, 291, and 292 covering sunspots *A* and *B*, shows a substantial nonthermal tail, consistent with thick target bremsstrahlung from fast electrons with a power-law spectrum $dJ/dE \sim E^{-\gamma}$ with γ between 6 and 6.5, J is the electron intensity at energy E. Such a spectrum must have a low energy cut-off at around 8 keV as the ratio of X-ray counts in the (3.5–5.5)/5.5–8.0) keV channels is incompatible with an extension to lower energies.

The 3.5–5.5 keV emission from the two pixels to the south of No. 271 and No. 291 is approximately 25% of the intensity of the latter. The HXIS subcollimators have a triangular response with maximum transmission at the geometric centre of a pixel, decreasing linearly to zero at the centre of adjacent pixels. A uniformly bright source exactly covering 1 pixel would have counts in the adjacent pixels of 6% (corner) and 19% (edge) of the counts in the source pixel*. This result from the early phase of the flare must therefore mean that only a small part, at most, of the X-ray emitting volume projects onto these pixels to the south, leading to the conclusion that the X-ray emission is coincident with the bright Hα kernel forming around sunspot *A*.

4.2. The period 22:38:30–22:39:30 UT

During this period, which is immediately prior to the first hard X-ray burst identified as *A* in Figure 3, the 3.5–5.5 keV intensity in No. 291 decreases, while it increases slowly in No. 292 and strongly in No. 272. The increase in No. 253, No. 273, and No. 293 is still quite low; by 22:39:30 UT the flux in No. 273 is only ~25% of that in No. 272, easily accounted for by the collimator response to a source in No. 272. Therefore the Hα kernel to the north of *B* is not, at this time, the site of a significant fraction of the X-ray output of the flare; neither is the arcade of loops stretching towards *D*. This is not surprising, as they are seen strongly in emission in Hα and therefore must be too cool to be seen in X-rays. The brightest point in this arcade, in X-rays, is No. 233, close to the NE end of the twisted pre-flare filament.

The relative behaviour of the X-ray intensity over the flaring pixels matches the motion of the bright Hα kernel around *A*. As the total emission is still rising without a corresponding drop in temperature, this motion must involve continuous energy release. However, in the next period the first large impulsive hard X-ray burst occurs, from which we deduce the detailed structure of the flare.

4.3. The period 22:39:30–22:41:00 UT

The first hard X-ray burst starts at the southern boundary of No. 272 and No. 292, as shown in Figure 8. This point is at the 'leading' edge of the Hα kernel as it rotates around *A*; in fact if our alignment is accurate to ~2″ it is just ahead of the advancing kernel. For the remainder of this time period we believe the development in X-rays is consistent with the expansion of the bulk of the energy released in this burst into a compact magnetic loop which may well be part of an arcade, linking the leading edge of the Hα kernel around *A* to the less intense kernel to the NW of *B*. In HXIS co-ordinates one of the loop footpoints lies at the south side of No. 272 and No. 292, approximately at the N–S boundary between them, and the other footpoint lies in the southern half of No. 273. The latter position is shown by the contour map between 22:40:58 UT and 22:42:00 UT in Figure 8. The loop footpoints are calculated to be ~14000 km apart,

* In principal the image can be corrected for this effect. The correction is straightforward if the source can be assumed to be pointlike, but for more complex structures the procedure becomes rather subjective; in general our images are not corrected for the collimator response unless stated.

allowing for foreshortening, which for semicircular geometry makes the top of the loop ~ 7000 km and the loop length $\sim 22\,000$ km. For the remainder of our discussion we will assume this physical picture is correct and interpret the observations accordingly.

The X-ray burst reached maximum intensity in No. 272 at around 22 : 39 : 45 UT (Figures 5 and 7), which compares with the local maximum of the total 22–30 keV intensity at 22 : 39 : 55 UT ± 5 s. The microwave burst at 17 GHz for the entire event reached a maximum intensity of 248 solar flux units at 22 : 39 : 54 UT (*Solar Geophysical Data*, 1981). Following the energy release at the southerly footpoint, the loop began to fill with hot, X-ray emitting plasma which produced increased emission in No. 273 and No. 293 until around 22 : 41 UT. The general increase in X-ray emission occurs at all energies imaged in HXIS, but in both these pixels the energy spectrum gradually softens, or cools, during the whole time period. However, the spectrum is always harder, or hotter, than that in No. 272. The loop clearly did not suddenly fill with fast electrons, otherwise there would be a similar impulsive hard X-ray burst from No. 273, the other footpoint.

The hard X-ray 'burst' in No. 273 is merely the high energy component of the thermal emission from the plasma in this region, which has been gradually heated by energy from the primary source in No. 272. The time between the onset of the hard X-ray burst in No. 272 to the maximum intensity in No. 273 is ~ 100 s. At a constant velocity, this would be $\pi R/100$ km s^{-1} with $R = 7000$ km, or ~ 200 km s^{-1}.

It is during this period that the peak in the magnetic transient occurs (Zirin and Tanaka, 1981), so it is appropriate to introduce our concept of the fields in the flare neighbourhood. Figures 10, a, b, c are a schematic representation of the magnetic fields at three stages of the flare, with Figure 10a describing this period. The magnetic transient is shown dotted and is attributed to an emerging bipolar region. Zirin and Tanaka detect a (conventionally) positive transient in a region of negative field but admit to the possibility that the transient is a dipole. The transient and compact flare loop are within a larger scale overlying magnetic field which plays no significant role at this stage. The instability that caused the initial energy release in the flare kernel which 'rotated' around sunspot *A* could either be the interaction of the emerging transient with the compact loop (e.g., model of Heyvaerts *et al.*, 1977) or it could result from changes in the degree of twist in the compact loop (e.g., model of Hood and Priest, 1980) driven by the forces which produce the transient. We interpret the disappearance of the transient as evidence for re-connection with some of the field lines of the compact flare loop, which then reinforce the overlying field.

Zirin and Tanaka (1981) refer to the substantial degree of left hand circular polarization of the 10.7 GHz radio burst, considerably higher than the polarization of the pre-flare emission. This sense of polarization arises from electrons moving in conventionally positive fields (Kai and Sheridan, 1974), which on our model would be from towards the *other* end of the compact loop. The radio data are not spatially resolved, and interpretation is difficult. However, the polarized radio emission is more probable from regions where the electron density is low, the mean free path is large, and the magnetic field strength high, whereas X-ray production necessarily requires the mean

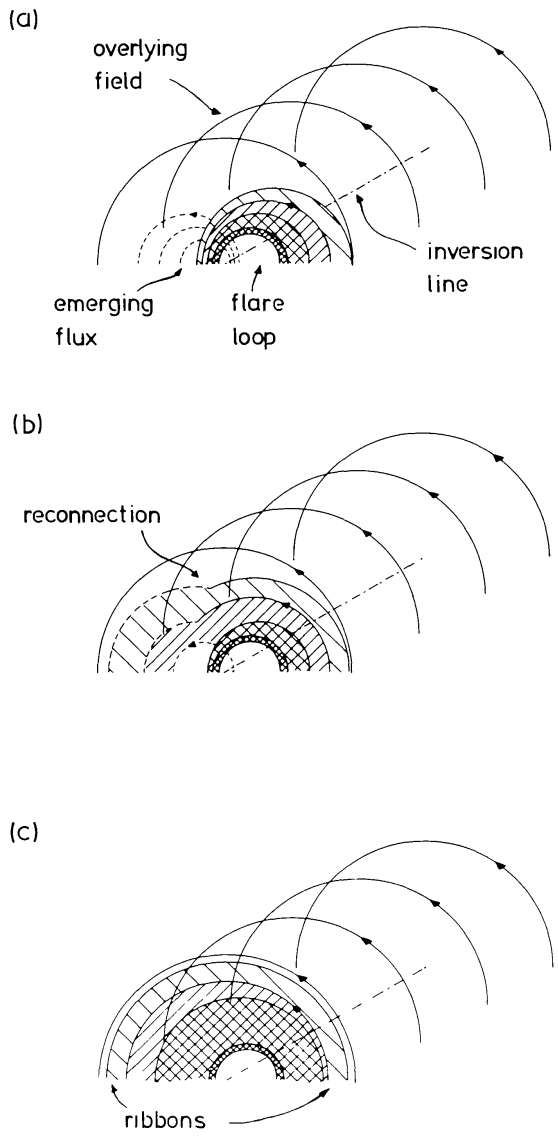

Fig. 10. A model showing our concept of the magnetic fields at different phases of the flare. (a) Around the time of the first hard X-ray burst. The emerging flux and the pre-existing flare loop start to interact. The overlying field is present as an arcade, but the smaller scale fields are envisaged as less extensive. The heavy cross hatching indicates the flux tube confining the bulk if the flare plasma. (b) After some reconnection, and energy release, has occurred. The higher altitude field lines of the flare loop have become part of the overlying field, but the bulk of the hot flare plasma is still confined to the cross hatched region. (c) The situation around 22:47 UT. The emerging flux has disappeared leaving a much simpler structure, where the volume available to the lighter cross hatched region has increased considerably. It is envisaged that the flare particules are diffusing into the single hatched regions, the base of which form the 2-ribbons observed in Hα.

free path to be small. Thus the X-rays are from the high density region near the reconnection area, while the radio emission is from less dense parts of the same magnetic loop. Polarization of radio sources in asymmetrical bipolar fields has been discussed by Kundu and Vlahos (1979), whose conclusions support our interpretation.

4.4. The period 22:41:00–22:42:30 UT

The second hard X-ray burst (*B* in Figures 3 and 7) occurs at 22:41:25 UT. The X-ray emission resulting from the first burst, at the lower energies imaged by HXIS, had started to fall in No. 273 and No. 293 when the second burst occurred. This burst appeared throughout the loop, indicating that, contrary to the first burst, the non-thermal electrons had rapid access to all parts of the loop. The bulk of the soft X-ray emission, containing the majority of the energy in the X-ray spectrum, remained at pixel No. 272.

Schematically, we believe the situation has evolved to that of Figure 10b, where the transient has weakened, the field strength or topology in the reconnection region has changed to allow the accelerated electrons free access to the whole of the compact loop, and the overlying field has become enhanced. The field strength of the compact loop has not diminished significantly and it can still contain the bulk of the flare plasma. We believe in this phase that chromospheric material expands into the compact loop, increasing the matter density and putting pressure on the magnetic field.

4.5. The period 22:42:30–22:45:00 UT

In this period we witness the gradual expansion of the hot plasma throughout the compact flare loop. The soft X-ray peak in No. 272 (Figure 9) occurs 10–15 s after the intensity in No. 273 and No. 293 have reached a minimum. For the next few minutes it appears that the X-ray emitting plasma merely becomes re-distributed throughout the loop. We do not believe there is any substantial fresh energy release, as examination of the spectrum in all four main pixels shows a monotonic cooling; also, the overall intensity in No. 273, No. 293, or No. 292 comes mainly at the expense of a decrease in No. 272. There is a slight altitude gain during this period, and the arguments advanced above regarding projection effects are equally true here to explain the behaviour of No. 293 relative to No. 273 and No. 272.

We may compute, as before, the time between the onset of the hard X-ray burst (*B*) and the second maximum in No. 273, at around 22:44:50 UT. This time is ~ 205 s, over double the time for the first burst; also, as the temperature in No. 273 is cooling throughout this period, maximum emission measure, which we correlate in this phase of the event with density, is still increasing. Therefore the time to maximum density is somewhat greater than this figure. If we interpret the re-distribution of plasma using diffusion theory, the density in the loop must have increased significantly to account for the relative slowness of the second event. This is discussed quantitatively by Simnett and Harrison (1983). Although we do observe a small altitude gain, it seems to be insufficient to imply that the delay could be purely due to a volume increase.

4.6. The period 22:45:00–22:50:00 UT

It is apparent from Figure 9 that although by $\sim 22:45$ UT the 3.5–5.5 keV X-ray intensity from No. 273 has also started to decline, emission from No. 293 is still rising to a broad maximum lasting until $\sim 22:50$ UT. We interpret this as clear evidence that the hot, X-ray emitting plasma is actually rising in altitude. As the plasma is cooling throughout this period the increased intensity in No. 293 can only be achieved through

a significant increase in emission measure. We show in Section 5 that the data suggest an expansion of material through the loop, which would account for the increase in emission measure. During this period, and the majority of the decay phase, the temperature derived for No. 293 for the higher temperature plasma (see Section 5) is consistently higher than that at the loop footpoints. This has been noted by de Jager *et al.* (1983) for a limb flare. Part of the increased emission measure could also represent an altitude increase of the loop, causing a larger fraction of it to project into pixel No. 293.

The altitude increase could be the result of diffusion of the plasma across field lines, or it could represent an expansion, or weakening, of the magnetic field in the compact loop. The latter could be brought about by progressive reconnection of field lines and/or increase in the plasma pressure. The former is more consistent with the model we are developing in Figure 10.

The most interesting event in this time period took place at $\sim 22:47$ UT, when, as we noted in Section 2, a distinct change in the Hα pictures occurred. In terms of the overall X-ray intensity, this event certainly did not contribute any extra flux (Figure 4). More significantly, the decay rates of both the low energy (e.g., 3.5–5.5 keV) and high energy (e.g., 22–30 keV) X-ray intensities change in *opposite senses*. The decay of the soft X-rays becomes more rapid, while the decay of the hard X-rays becomes slower; remember that the flare developed as a 2-ribbon flare from this point. The change in the Hα picture was most apparent around sunspot *A*, where the kernel appeared to break with the bright plage ribbon extending southwards; it then 'crossed' over the sunspot and re-joined the plage ribbon. This event clearly signals a critical stage in the flare evolution and we interpret it in the following way:

(1) For the duration of the main phase of the flare, all the flare energy has been confined to a relatively compact loop structure whose footpoints are in No. 272 and No. 273. Cooling times are a function of the physical parameters of this loop, which is not stationary, but is gradually expanding upwards.

(2) The presence of the emerging flux (the transient) causes continuous reconnection which weakens the magnetic field in the compact loop until it can no longer contain the flare plasma.

(3) The plasma expands into the larger volume defined by the overlying field (Figure 10c) whose footpoints are rooted at the location of the bright Hα ribbons. The flare energy now manifests itself at photospheric level via the ribbons, rather than the more compact kernels seen up to this point. This expansion leads to an increase in the decay rate of the softer (3.5–5.5 keV) X-ray emission.

(4) The simultaneous change in decay rates of the low and high energy X-rays, but in opposite senses, is intriguing. If the emissions are thermal, this behaviour would indicate a multithermal plasma where the high temperature components had the slowest decays. This would suggest an environment where the cooling was radiation-dominated. As the relative cooling times between a conduction-dominated and radiation-dominated plasma at temperature T, contained in a magnetic loop of length L and electron density n_e vary as $L^2 n_e^2 T^{-7/2}$ (Moore *et al.*, 1980), the observations would be consistent with an expansion to a lower density state.

An alternative explanation is that the X-rays > 22 keV are partly bremsstrahlung from a non-thermal distribution of electrons. It is possible to interpret the X-ray time profile in Figure 3 as the superposition of impulsive, fast decaying bursts (the last being at 22 : 46 UT) on top of a slowly varying base-level, and a slowly varying increase starting around 22 : 45 UT, reaching maximum at 22 : 50 UT. Microwave radio activity occurred predominantly at the times of the impulsive bursts, while a metric type II burst was observed by Culgoora (22 : 44–22 : 55 UT) and Harvard (22 : 48–22 : 55 UT) (*Solar Geophysical Data*, 1980). We would therefore interpret the slowly varying burst, predominant after 22 : 47 UT, as arising from electrons accelerated by the disturbance responsible for the type II burst and contained in the overlying magnetic structure.

4.7. The period 22 : 50 : 00–23 : 08 : 00 UT

This is the last period we discuss here. The previously dominant pixels No. 272 and No. 273 continue to decay and remain the site of the majority of the X-ray emission. There is now increasing flux from No. 254 and No. 274. We interpret this as emission from the top of the new loop system linking the two Hα ribbons. These lie in the NE–SW direction, and following the reconfiguration at 22 : 47 UT the intensity in No. 234 quickly rose to a maximum. As the pixels along the axis of the arcade of loops at photospheric level decay, those to the NW, namely No. 254, No. 274, No. 293, and No. 292 show enhanced emission with respect to the 'axis' pixels. This is consistent with an altitude increase, as discussed above. The loops are apparently still growing at the end of the time period, as the emission in No. 292 and No. 293 increases at ~ 23 : 05 UT.

The soft X-ray results from Skylab (Vorpahl *et al.*, 1975) showed that flares were most commonly observed at several loops in an arcade. The event here is not inconsistent with this observation; however, our good time resolution shows that the *initial* release, plus the development for minutes afterwards, is in one loop and only in the later stages of the flare are X-rays observed throughout the whole arcade.

5. Derivation of the Physical Parameters

We have measured the X-ray intensity as a function of time, energy and position in a compact flare. Comparison of the Hα and X-ray data has allowed us to suggest a spatial structure for the core of the event which is consistent with the observations. With this information, we can apply standard modelling results to calculate the X-ray emission measure as a function of temperature, the electron density and the number of non-thermal electrons in the hard X-ray burst.

A critical part of the interpretation is that the hard X-ray emissions at the times shown in Figure 6 are concentrated at different ends of a compact magnetic loop. Furthermore, the compact nature of the source suggests an upper limit to the diameter of the flux tube of 6000 km, with the best value at 4500 km. From considerations of projection due to the location at N 29 W 29, the inferred altitude is in the range 7000–10 000 km and the

loop footpoints are separated by $\sim 14\,000$ km. From these data the volume of the loop is in the range 3.5×10^{26} cm^3–5.5×10^{26} cm^3.

The temperature structure, and the time evolution of the temperature and density of the loop, are discussed in depth by Simnett and Harrison (1983). It is not within the scope of the current paper to discuss their results in detail, but it is nevertheless useful to indicate how such analysis can support the model proposed here. Table I gives preliminary results for three time periods in this flare: (a) the peak of the first hard X-ray burst; (b) the peak of the soft X-ray intensity in pixel No. 272; and (c) a point on the decay. We now outline the analysis technique.

HXIS measures the X-ray luminosity of the flaring pixels simultaneously in six energy bands. In this flare, over integration times of around half a minute statistically significant counting rates (around 10% counting statistics, or better) are obtained in the lowest four energy bands. The HXIS counting rate prediction program (see Boelee (1983), based on theoretical predictions of Gronenschild and Mewe (1978)) is used to predict the distribution of counts in each energy band for each pixel as a function of the temperature and emission measure of the plasma imaged by that pixel. In principle a differential emission measure analysis can be performed, although in practice we are limited by the finite number of energy channels with statistically significant counting rates. There is significant emission in this flare at temperatures in the $25–30 \times 10^6$ K region, with a substantial residual component at lower temperatures. The data presented in Table I are from a two temperature analysis wherever the counts have statistical significance. The high temperature component is derived from the relative counting rates in the (8.0–11.5 keV)/(11.5–16 keV) channels (although in the detailed analysis all 6 energy bands are used), and the predicted counts from this component in the 3.5–5.5 keV and 5.5–8.0 keV channels (1 and 2) are subtracted from the low temperature component, with a second iteration if the low temperature component predicts significant counts in the 8.0–11.5 keV interval. Where the low temperature component is absent this indicates that the residual counts in channels 1 or 2 after subtraction of the 'best fit' high temperature component were less than the 1σ uncertainty in the original count.

The preliminary results are supportive of the model outlined above to account for the flare development. For the purpose of deriving the electron density, n_e, in Table I the volume of the loop is taken as 3.5×10^{26} cm^3, imaged by the four pixels in the following proportions: No. 272 – 30%; No. 292 – 20%; No. 293 – 15%; No. 273 – 35%. During the first hard X-ray burst, the density at the flaring footpoint is enhanced with respect to the density at the other footpoint, indicating that some chromospheric material may have expanded into the loop. Following the second burst, the density appears to be considerably enhanced at the flaring footpoint and in the decay phase the density at this footpoint decreases while it increases at the other footpoint. This would be consistent with the transfer of hot material around the loop. In all periods and at all points the emission measure at the higher temperature is less than that at the lower temperature by $\sim$ two orders of magnitude.

We may also estimate the number of energetic electrons needed to account for the first hard X-ray burst on the assumption of thick target emission. Using the results of

TABLE I

Temperatures and emission measures at three phases of the flare using a two-temperature model. The temperatures are accurate to $\approx 3\%$ within the constraints of the model. All other parameters are model dependent and should be interpreted only as a guide to the physical situation.

Period	22:39:50–22:40:27 UT			22:42:54–22:43:31 UT			22:44:44–22:45:21 UT		
Pixel	Temperature 10^6 K	Emission measure 10^{48} cm^{-3}	Density n_e – cm^{-3}	Temperature 10^6 K	Emission measure 10^{48} cm^{-3}	Density n_e – cm^{-3}	Temperature 10^6 K	Emission measure 10^{48} cm^{-3}	Density n_e – cm^{-3}
272	30 7.0	2.2 195	1.4×10^{12}	24 5.3	12.3 2300	4.7×10^{12}	25 6.4	7.1 790	2.7×10^{12}
292	30 6.7	1.4 130	1.4×10^{12}	27 5.3	3.7 560	2.8×10^{12}	26	4.2	
273	30 7.5	1.8 79	8.1×10^{11}	26 7.3	3.5 84	8.3×10^{11}	26 7.2	5.1 160	1.2×10^{12}
293	33 6.7	0.5 54	1.0×10^{12}	26	1.4		26	1.8	

thick target bremsstrahlung calculations (e.g., Brown, 1971; Petrosian, 1973; Langer and Petrosian, 1977) we calculate the number of electrons, above 16 keV, required as $\sim 3 \times 10^{36}$ s^{-1} at the peak of the burst. If we require such a beam to persist for ~ 60 s, this results in $\sim 5 \times 10^{30}$ erg total kinetic energy in such electrons. As pointed out by Lin and Hudson (1971) some years ago, this energy may well represent the major fraction of the total flare energy budget, with the thermal phase of the flare deriving its energy from the electrons.

6. Conclusions

The results of this study have focussed on the identification of a compact loop within the flare region as the site of the main energy release. During the periods of impulsive hard X-ray emission the flare, in Hα, appeared principally as two bright kernels, one of which was dominant. These merely represent the footpoints of the magnetic flux tube delineating the prime flare activity and do not themselves indicate the site of the energy release. In the second hard X-ray burst we observe non-thermal emission from both footpoints, simultaneously, within the coarse* time resolution of the measurements. This behaviour has been noted from earlier HXIS results on different flares (Hoyng *et al.*, 1981; Duijveman *et al.*, 1982). The significant results from this study are the following:

(1) The primary exothermic reaction occurs near one of the loop footpoints. We believe, for this flare, that this answers the question posed recently by Moore *et al.* (1980) as to the point at which the flare plasma is heated.

(2) The energy source is consistent with interaction of emerging flux, seen as a magnetic transient by Zirin and Tanaka (1981) with the preexisting compact magnetic loop in the manner outlined by Heyvaerts *et al.* (1977). (On account of the 'rotation' of the principal Hα kernel, it might be practical to consider the twisted loop model of Hood and Priest (1979, 1981) as an alternative.) Whether the emerging flux manifests itself as a transient or a new sunspot (as in the May 21 flare; see Hoyng *et al.*, 1981) is merely a question of the relative strengths of the emerging and existing magnetic loops.

(3) The principal energy release at one end of the loop causes expansion of chromospheric material into the loop, leading to an increase in density. There is evidence, following the second major energy release, that hot plasma expanded throughout the loop, causing an increasing in density at the other footpoint. This is consistent with ideas first expressed by Neupert (1968).

(4) The subsequent development of the flare, as seen in Hα, as a 2-ribbon flare is a function of the topology of the overlying magnetic field which appears to play no role in the evolution of the early, impulsive stages of the flare. We believe this event shows that the development of the Hα flare as 2 ribbons is entirely a secondary process, powered by the energy liberated in the impulsive phase. It has been noted (Švestka, 1976) that the ribbons in a 2-ribbon flare generally separate. This is entirely consistent with the model presented in Figure 10, where the hot material gradually expands into

* Coarse when compared with the transit time of 30 keV electrons around the loop.

higher parts of the overlying magnetic arcade, whose footpoints are consequently further and further apart.

(5) The first impulsive hard X-ray burst is consistent with nonthermal bremsstrahlung from an electron population of 3×10^{36} electrons s^{-1} above 16 keV. The total energy in these electrons is $\sim 5 \times 10^{30}$ erg. The second burst is smaller but of comparable magnitude.

(6) The hottest temperatures are generally seen at the top of the compact loop. This is especially true during the relatively long delay phase of the event. This is consistent with HXIS results on other flares (e.g., de Jager *et al.*, 1983). Possible contributions to this effect from non-thermal emission cannot be eliminated. Skylab results in the soft X-ray region (Pallavicini and Vaiana, 1976; Pallavicini *et al.*, 1975) quite definitively showed that the looptops were the hottest part of the post-flare structure.

(7) The altitude of the top of the flaring loop is between 7000 and 10000 km, and appears to increase as the flare proceeds. Expansion of flare structures has been known for many years from ground based observations of limb flares (Severny and Shaposhnikova, 1960). In the July 5 event, we have been able not only to investigate the development of the flare in Hα but also to follow the position of the more energetic phenomena as seen in X-rays. A somewhat similar study, made on June 25, 1980 with the same objectives, has recently been reported by Kundu *et al.* (1982) in which the Hα data are compared with microwave observations with the Very Large Array of the National Radio Astronomy Observatory. It is believed that the microwave data originates from electrons ~ 100 keV; consequently, if the same event were studied with Hα, HXIS, and the VLA we would have imaging capability representative of the electron distribution in three different electron energy regimes, each representing a fundamentally different viewpoint of the flare.

Acknowledgements

The development and construction of the Hard X-Ray Imaging Spectrometer, principal investigator Prof. C. de Jager, was made possible by support given by the Netherlands Ministry for Education and Science through the Committee for Geophysics and Space Research of the Royal Netherlands Academy of Arts and Sciences, and the Science Research Council (now the Science and Engineering Research Council) of the United Kingdom. The mechanical construction was achieved under the direction of H. LaFleur and the on-board software was developed by Dr R. J. Fryer and G. Wiersma.

We are grateful to Dr B. R. Dennis for his critical reading of an early version of the manuscript. We thank Prof. H. Zirin for making the Big Bear Hα photographs available to us; Dr J. Schrijver, M. Galama, and F. Werkhoven for their contributions to the software; and many members of the SMM team for useful discussions. R.A.H. is grateful to the Science and Engineering Research Council for a research studentship.

Appendix: The HXIS/Hα Alignment

Prior to the large flare of 22 : 30 UT, HXIS observed two smaller events; one at 16 : 14 UT and one at 18 : 35 UT. We will use the data from these two events to make the alignment.

In Hα at 16 : 02 UT, two patches of emission were clearly visible from Active Region 2550. The more intense patch was along the north–western edge of sunspot *A* Figure 1b, and weaker emission was observed to the south of area *F*. From the first minute of Sun, at 16 : 14 UT, HXIS observed two patches of emission as well. Once again, one was more intense. In the HXIS field of view, their distance of separation was similar to the separation of the two Hα patches. By 16 : 14 UT, the more intense patch had formed into a two-ribbon system.

The 18 : 35 UT event was of minor importance, but it was very compact in Hα, being immediately to the north–west of sunspot *A*. No other emission was observed from the region. This was a subflare; it did not develop into a two-ribbon system and was short lived. At this time, HXIS also saw one compact patch of low intensity emission.

Since the latter event was so compact, we will assume that the Hα and soft X-rays originated from the same point. The location of this emission appears to be very low in the atmosphere. No loop system or large structure of any kind is inferred from the Hα data. In the 16 : 14 UT event, the X-rays probably originated higher in the atmosphere since the Hα clearly defines a series of large loops.

In Figure A1a, the HXIS and Hα data have been aligned, with the above assumption for the 18 : 35 UT subflare event. In the NE–SW direction, the accuracy is probably to

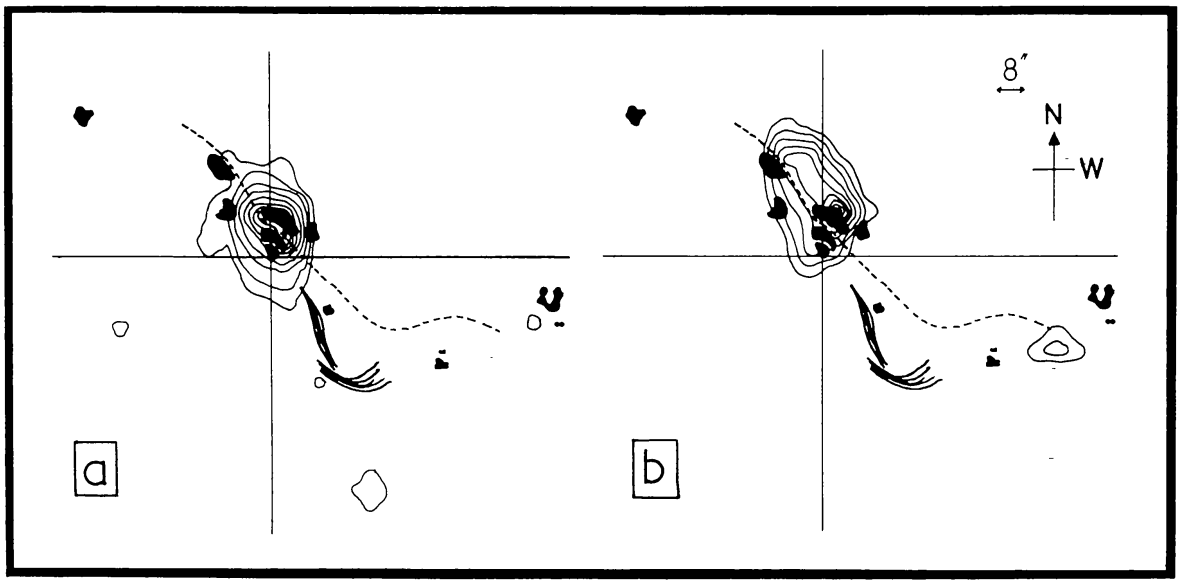

Fig. A1. (a) A contour map of the 18 : 35 UT subflare event as observed by HXIS overlayed onto the active region, assuming the Hα and soft X-ray emission to be colocated. The contour levels are at 98, 90, 80, 70, 55, 40, 26, 14, and 7%. The image is corrected for the triangular response of the collimator. (b) An overlay for the 16 : 18 UT flare assuming the Figure A1a alignment to be correct. The contours are at the same levels as Figure A1a and the image is again corrected.

better than 4″, since the patches in Hα and as seen by HXIS, are so compact. For the NW–SE direction, since the region is in the north–west solar quadrant, the error can only be to the NW due to a height difference, but because of the nature of this event, this can only be small, probably less then a few arc sec.

Assuming Figure A1a to be correct, Figure A1b shows the 16 : 14 UT flare alignment. In this case, the central patch implies a height offset of less than 8″, giving a flare altitude of $\sim 10^4$ km. This is consistent with height calculations for the 22 : 30 UT flare event, which had a similar structure in the later stages.

The south–western patch, as seen in Figure A1b, is also consistent with the Hα data if the source has a lower altitude than the main patch, as no offset is observed. This seems likely since no loop structures are seen in Hα, merely plage brightenings. The observation of these two patches also confirms the spacecraft roll angle as being zero.

References

Boelee, A.: 1983, Thesis, Space Research Lab., Utrecht.

Brown, J. C.: 1971, *Solar Phys.* **18**, 489.

de Jager, C. and de Jonge, G.: 1978, *Solar Phys.* **58**, 127.

de Jager, C., Fryer, R. J., Hoyng, P., LaFleur, H., Schadee, A., Simnett, G. M., Švestka, Z., Van Beek, H. F., and Van Tend, W.: 1981, *Adv. Space Res.* **1**, 251.

de Jager, C., Machado, M. E., Schadee, A., Strong, K. T., Švestka, Z., Woodgate, B. E., and Van Tend, W.: 1983, *Solar Phys.* **84**, 205 (this volume).

Duijveman, A., Hoyng, P., and Machado, M. E.: 1982, *Solar Phys.* **81**, 137.

Gronenschild, E. H. B. M. and Mewe, R.: 1978, *Astron. Astrophys. Suppl.* **32**, 283.

Heyvaerts, J., Priest, E. R., and Rust, D. M.: 1977, *Astrophys. J.* **216**, 123.

Hood, A. W. and Priest, E. R.: 1979, *Solar Phys.* **64**, 303.

Hood, A. W. and Priest, E. R.: 1980, *Solar Phys.* **66**, 113.

Hood, A. W. and Priest, E. R.: 1981, *Solar Phys.* **73**, 289.

Hoyng, P., Duijveman, A., Machado, M. E., Rust, D. M., Švestka, Z., Boelee, A., de Jager, C., Frost, K. J., LaFleur, H., Simnett, G. M., Van Beek, H. F., and Woodgate, B. E.: 1981, *Astrophys. J.* **246**, L155.

Kai, K. and Sheridan, K. V.: 1974, *Solar Phys.* **35**, 181.

Kundu, M. R. and Vlahos, L.: 1979, *Astrophys. J.* **232**, 595.

Kundu, M. R., Schmahl, E. J., and Velusamy, T.: 1982, *Astrophys. J.* (in press).

Langer, S. H. and Petrosian, V.: 1977, *Astrophys. J.* **215**, 666.

Lin, R. P. and Hudson, H. S.: 1971, *Solar Phys.* **17**, 412.

Lin, R. P. and Hudson, H. S.: 1976, *Solar Phys.* **50**, 153.

Moore, R., McKenzie, D. L., Švestka, Z., Widing, K. G., and 12 co-authors: 1980, in P. A. Sturrock (ed.), *Solar Flares*, Colorado Associated University Press.

Neupert, W. M.: 1968, *Astrophys. J.* **153**, L59.

Pallavicini, R. and Vaiana, G. S.: 1976, *Solar Phys.* **49**, 297.

Pallavicini, R., Vaiana, G. S., Kahler, S. W., and Krieger, A. S.: 1975, *Solar Phys.* **45**, 411.

Petrosian, V.: 1973, *Astrophys. J.* **186**, 291.

Severny, A. B. and Shaposhnikova, E. F.: 1960, *Izv. Krymsk, Astrofiz. Obs.* **24**, 235.

Simnett, G. M. and Harrison, R. A.: 1983, in preparation.

Solar Geophysical Data: 1980, September, No. 433, Part I.

Solar Geophysical Data: 1981, January, No. 437, Part II.

Švestka, Z.: 1976, *Solar Flares*, D. Reidel Publ. Co., Dordrecht, Holland.

Van Beek, H. F., Hoyng, P., LaFleur, H., and Simnett, G. M.: 1980, *Solar Phys.* **65**, 39.

Vorpahl, J. A., Gibson, E. G., Landecker, P. B., McKenzie, D. L., and Underwood, J. H.: 1975, *Solar Phys.* **45**, 199.

Zirin, H. and Tanaka, K.: 1981, *Astrophys. J.* **250**, 791.